Magnetic Nanochains of $FeNi_3$ Prepared by a Template-Free Microwave-Hydrothermal Method

Juncai Jia,[†] Jimmy C. Yu,*[,†] Yi-Xiang J. Wang,[‡] and King Ming Chan[§]

Department of Chemistry, Environmental Science Programme, and Centre of Novel Functional Molecules, Department of Imaging and Interventional Radiology, Prince of Wales Hospital, and Department of Biochemistry and Environmental Science Program, The Chinese University of Hong Kong, Shatin, New Territories, Hong Kong, China

ABSTRACT Magnetic $FeNi_3$ nanochains were synthesized by reducing iron(III) acetylacetonate and nickel(II) acetylacetonate with hydrazine in ethylene glycol solution without any template under a rapid and economical microwave irradiation. The morphology and composition of the as-prepared products were characterized by field-emission scanning electron microscopy (FESEM), transmission electron microscopy (TEM), X-ray diffraction (XRD), and elemental mapping. The size of the aligned nanospheres in the magnetic $FeNi_3$ chains could be adjusted from 150 to 550 nm by increasing the amounts of the precursors. The length of the nanochain is about several tens of micrometers. The ratio of the precursors plays an important role in the formation of $FeNi_3$ nanostructures. Magnetic measurement reveals that the $FeNi_3$ nanochains show enhanced coercivity and saturation magnetization. The formation mechanism of the product is discussed. Toxicity tests of $FeNi_3$ nanochains show that the as-prepared nanochains are nontoxic to zebrafish larvae. *In vitro* magnetic resonance imaging (MRI) confirms the effectiveness of the $FeNi_3$ nanochains as sensitive MRI probes.

KEYWORDS: iron−nickel alloy • nanochains • microwave irradiation • toxicity • magnetic resonance imaging

1. INTRODUCTION

One-dimensional (1D) nanostructures have drawn great attention in recent years because of their distinctive geometries and special optical, photoelectric, and electrochemical properties (1−6). In particular, 1D magnetic nanochains have stimulated interests in many research fields such as electrical transport, magnetic switching (7), magnetotransport behavior (8), micromechanical sensors (9), DNA separation, and other biomedical applications (10−12). In comparison to the zero-dimensional nanoparticles, 1D nanochains provide more parallel-aligned surface functionalities per molecular structure, which are suitable for multivalent molecular recognition on cell surfaces (12). Macrophage cells may take up the 1D nanochains more rapidly than nanoparticles by their differences in mass (13). Transition metal alloys have been extensively studied in the past several decades for their increasing utility in electronic and energy conversion devices (14). Alloys form when two or more metals coaggregate to produce compositionally ordered structures, with properties that differ from those of bulk alloys or nanoparticles of the individual components (15−18). This makes magnetic alloy nanoparticles particularly interesting because of their high saturation magnetization (19) and resistance against oxidation (20). As important transition alloys, iron−nickel alloys, such as $FeNi_3$, are of great interest because of their useful magnetic properties and wide applications (21−25). Owing to the distinctive 1D intrinsic anisotropic shape, comparing to the zero-dimensional nanoparticles, these $FeNi_3$ nanochains are expected to exhibit enhanced magnetic coercivity and saturation magnetization and can be used as a new class of MRI probes with high sensitivity. However, until now, there have been only several methods to prepare the $FeNi_3$ nanoparticles, such as electrical explosion of wire (22) and chemical reduction using hydrazine in aqueous solutions (23−25). The methods reported are either time-consuming, or they require additional surfactant or template. And the reported $FeNi_3$ does not have a regular shape or an ordered structure.

Herein, we report a rapid and economical microwave-assisted approach to fabricate awaruite $FeNi_3$ nanochains in ethylene glycol solution in one step (see Scheme 1). Microwave irradiation is an efficient process that becomes an increasingly popular heating method for nanomaterials synthesis (26−28). We have successfully synthesized colloidal Fe_2O_3 nanocrystals (29), carbon-based interconnected cablelike Ag/C (30), Ni nanowires (31), and superparamagnetic porous Fe_3O_4/C nanocomposites (32) by taking advantage of microwave irradiation and hydrothermal effects. In this work, the $FeNi_3$ nanochains were synthesized within several minutes without using any hard templates or catalysts. The structure, morphology, and composition of the nanochain products are investigated by changing the experiment conditions, such as the amounts of precursors, the

* Corresponding author.
Received for review May 11, 2010 and accepted July 27, 2010
[†] Department of Chemistry, Environmental Science Programme, and Centre of Novel Functional Molecules, The Chinese University of Hong Kong.
[‡] Department of Imaging and Interventional Radiology, Prince of Wales Hospital, The Chinese University of Hong Kong.
[§] Department of Biochemistry and Environmental Science Program, The Chinese University of Hong Kong.
DOI: 10.1021/am100410r

Scheme 1. Illustration of a Proposed Mechanism for the Formation of $FeNi_3$ Nanochains

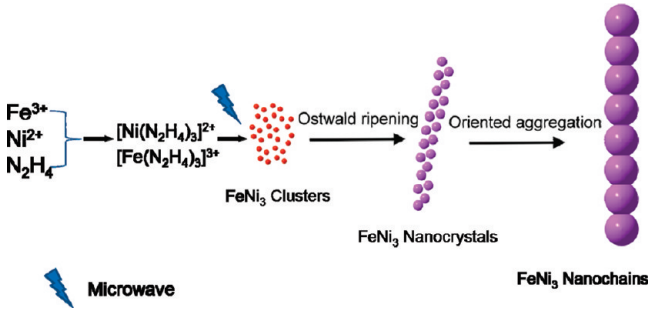

relative ratio of Fe and Ni precursors and the solvent. The toxicity of the product is tested by exposing the zebrafish larvae to the product solution. And the potential contrast relaxivity of the product as the MRI probes is also studied. It is expected that the unique shape of these nanostructures can find applications for cell labeling, as drug carrier, magnetic separation of labeled cells and other biological entities, and in the application of magnetic targeting (13).

2. EXPERIMENTAL SECTION

Reagents. Iron(III) acetylacetonate ($Fe(acac)_3$, 95%), nickel(II) acetylacetonate ($Ni(acac)_2$, 95%), ethylene glycol (EG, 99.8%), triethylene glycol (TEG, 99%), hydrazine monohydrate (98%) were supplied by Aldrich. Deionized water was used throughout. All chemicals were used as received without further purification.

Synthesis of Necklacelike $FeNi_3$ Nanochains. All the samples were prepared in a microwave digestion system (Ethos TC, Milestone). The detailed conditions are listed (see Table 1 in the Supporting Information). In a typical procedure, 0.07 mmol iron(III) acetylacetonate and 0.2 mmol nickel(II) acetylacetonate were dissolved into 45 mL ethylene glycol, and then 1 mL of hydrazine monohydrate was added dropwise by an autopipette over a 1 min period. After stirring mildly for about 5 min, the solution was sealed in a high-pressure digestion vessel that was Teflon-lined and double-walled. The reaction vessel was fitted with a temperature probe that was housed in a sturdy thermowell and protected from chemical attack by a triple layer of PTFE/ceramic/PTFE. The desired exposure time and temperature were programmed by using Milestone's EasyControl software. The Automatic Temperature Control system allowed continuous monitoring and controlling (±1 °C) of the internal temperature. The preset profile (desired time and temperature) was followed automatically by continuously adjusting the applied power (0−1000 W). After treating the mixture at 160 °C for 5 min under microwave irradiation, the vessel was cooled to room temperature. The product was collected, washed with deionized water and absolute ethanol, and dried in a vacuum at 60 °C for 4 h.

Characterization of Necklacelike $FeNi_3$ Nanochains. The general morphology of the products was characterized by a field-emission scanning electron microscope (FESEM, FEI, Quanta 400 FEG). Transmission electron microscopy (TEM, FEI/PHILIPS CM120), high-resolution TEM (HRTEM), and high angle annular dark field scanning TEM (HAADF-STEM) measurements were carried out on a Tecnai F20 microscope (FEI, 200 kV) coupled with an HAADF detector and an energy-dispersive X-ray (EDX) spectrometer. Two-dimensional STEM-EDX elemental mapping was performed for the $FeNi_3$ product. The electron probe size for the STEM-EDX analysis was about 1 nm. X-ray diffraction (XRD) patterns were collected using a Bruker D8 Advance diffractometer using Cu Kα irradiation ($\lambda = 1.5406$ Å). Powdered products were weighed out for magnetic characterization by vibrating sample magnetometry (VSM-7300, Lakeshore, U.S.A.).

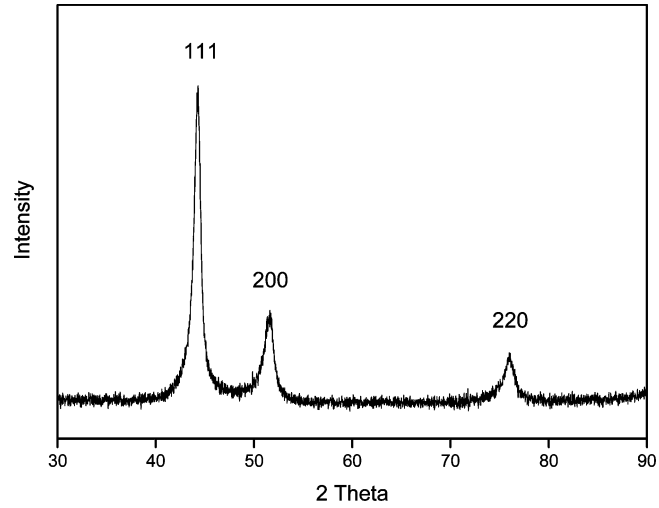

FIGURE 1. XRD patterns of the as-prepared $FeNi_3$ nanochains (S1).

Toxicity Test—Exposure of the Zebrafish (*Danio rerio*) Larvae to $FeNi_3$ Nanochains. For toxicity studies, 20 healthy zebrafish larvae (5 day postfertilization and hatched) were transferred to a 100 mL polyethylene beaker containing 50 mL of a solution prepared by dissolving 60 mg of artificial sea salt in one liter of ultrapure (deionized and purified after reverse osmosis) water. All fish rearing conditions and larval production procedures were carried out according to Westerfield (33) and the bioassay was performed according to the OECD recommended method (34). Graded concentrations of $FeNi_3$ nanochains (0, 1, 5, 10, 25, 35, 50 mg/L) were sonicated and incubated for 96 h at 28.5 °C. Tests were performed in triplicate and repeated twice (120 larvae per concentration). The survival rate is expressed as the total number of survival larvae after 24, 48, and 96 h.

***In vitro* MRI of $FeNi_3$ Nanochains.** MR relaxometry of the $FeNi_3$ nanochains was performed using a clinical 1.5 T whole-body MR system (Siemens Sonata, Erlangen, Germany) in combination with a knee radio frequency coil for excitation and signal reception. $FeNi_3$ nanochains were dispersed in distilled water at iron concentrations ranging from 0 to 0.2 mmol/L. For MR measurements, $FeNi_3$ nanochains dispersed solutions (1 mL) were filled in each 1.5 mL Eppendorf tubes. Sonication was applied for 10 min prior to MRI using at 40 kHz (Branson 3510E-MTH) in water at ambient temperature. T_2 relaxation times were measured using a standard Carr-Purcell-Meiboom -Gill pulse sequence (TR = 2000 ms, TE range = 30−960 ms, 32 echoes, FOV = 134 × 67 mm, matrix = 128 × 64, slice thickness = 5 mm, NEX = 3). T_2 relaxation times were calculated by a linear fit of the logarithmic ROI signal amplitudes versus TE. The T_2 relaxivity (r_2) was determined by a linear fit of the inverse relaxation times as a function of the iron concentrations used.

3. RESULTS AND DISCUSSION

Black powders were obtained from the microwave-assisted reaction of ethylene glycol iron(III) acetylacetonate and nickel(II) acetylacetonate. Figure 1 shows the X-ray diffraction (XRD) pattern of a typical product. All peaks can be indexed to the awaruite $FeNi_3$ alloy, which is in good agreement with the reported data (Joint Committee on Powder Diffraction Standards, JCPDS card no. 38−0419). No iron and nickel oxides, hydroxides or other impurities phases are detected. The sharp peaks and the low back-

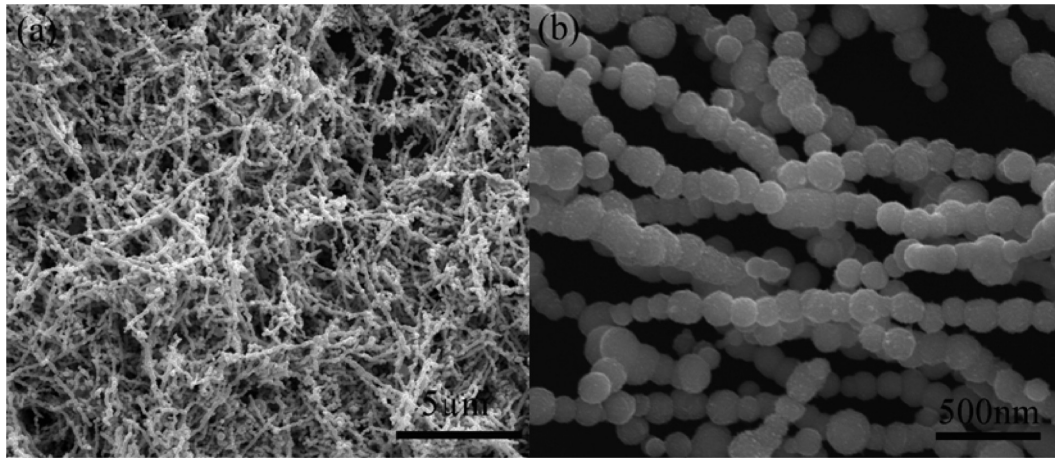

FIGURE 2. (a) Low- and (b) high-magnification FESEM images of S1.

ground reveal that the as-synthesized iron−nickel alloy particles had a high degree of crystallinity. This indicates that well-crystallized $FeNi_3$ nanochains can be easily obtained under the proposed preparation conditions.

The morphology of the as-obtained products was characterized by FESEM and TEM. A general overview FESEM image in Figure 2a shows that the product is composed of nanochains with a diameter of 150 nm and length about several tens of micrometers. Enlarged FESEM images (Figure 2b) show that the nanochains are comprised of many aligned nanospheres. Representative TEM images (Figure 3a) clearly show the shape of necklacelike nanochains, and a high-magnification TEM image (Figure 3b) shows that the chain is necklacelike and the diameter of each nanosphere is about 150 nm. An electron diffraction (ED) pattern (Figure 3c) was recorded by focusing the electron beam on an individual nanochain. The results suggest that the products are polycrystalline. Figure 3d shows a HRTEM image at the edge of an individual $FeNi_3$ nanosphere. As shown in Figure 3d, a typical intensity profile covers the line scan (labeled by a line in Figure 3e) across the lattice fringes. The periodic fringe spacing of ~2.0 Å agrees well with interplanar spacing between the {111} planes of the awaruite $FeNi_3$. The local elemental composition of the as-formed nanochains was studied by EDX microanalysis at the single-nanochain level, shown in Figure 4. It confirms that the nanochains are composed of Fe and Ni elements. Figure 5a−d show the typical high angle annular dark field scanning TEM (HAADF-STEM) and EDX elemental mapping images of an individual nanochain. The results confirm the existence of Fe and Ni elements, which are distributed homogenously over the entire nanochains.

The magnetic properties of the products were characterized by VSM. Figure 6 shows the room-temperature magnetization hysteresis loop. Clearly, it reveals a typical ferromagnetic behavior with saturation magnetization (Ms) of 53.6 emu g^{-1} and coercivity field (Hc) of 53.0 Oe. The hysteresis curve is symmetric in shape with respect to zero magnetic field. It is worth noting that the $FeNi_3$ nanochains exhibit significantly enhanced magnetic coercivity (about 100 times higher) compared with that of bulk $FeNi_3$ (0.54

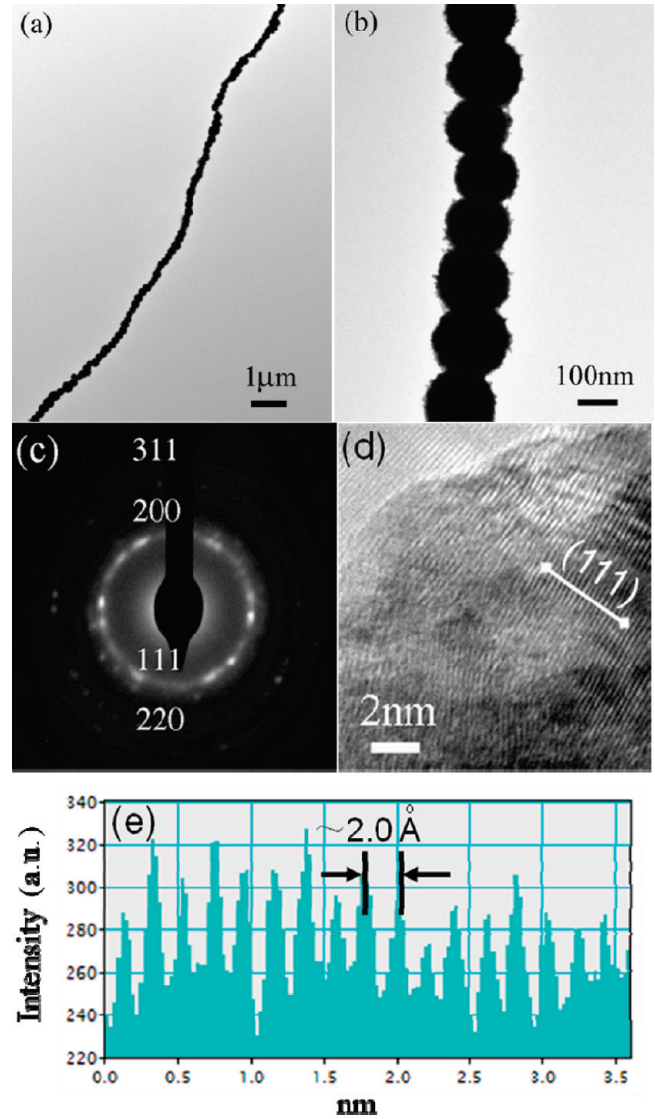

FIGURE 3. (a, b) Bright-field TEM and enlarged TEM image of S1. (c) ED pattern indicating the polycrystalline nature of the nanochains. (d) Typical HRTEM image. (e) Corresponding intensity profile for the line scan across the lattice fringes.

Oe), and the saturation magnetization is about 350 times higher than the monodispersed $FeNi_3$ nanospheres (0.15 emu g^{-1}) (23). This may be ascribed to the distinctive 1D

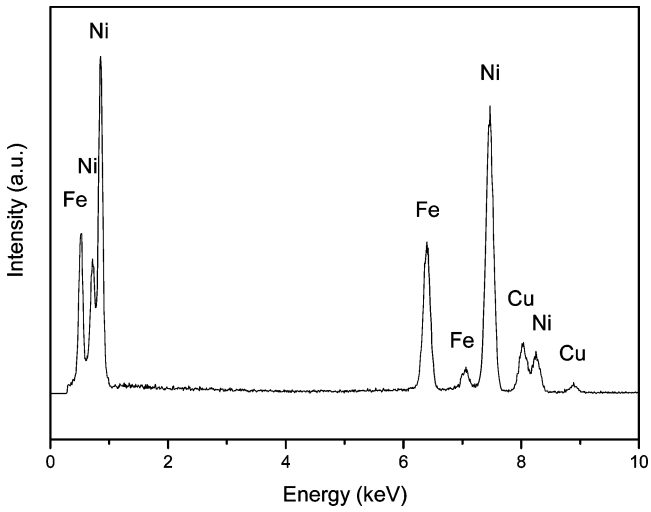

FIGURE 4. EDX spectrum of a single $FeNi_3$ nanochain from S1, where the signals of Cu are generated from the Cu grids.

anisotropic structure and hierarchical surfaces of the magnetic nanochains. Figure 7 also shows a fast response to a foreign magnet and can be rapidly separated from the solution.

We further investigated the effects of reactant concentration and solvents on the morphology of the $FeNi_3$ products. Results are summarized in Table 1 of Supporting Information. The amounts of $(Fe(acac)_3$:$Ni(acac)_2)$ had a significant effect on the size of the as-prepared $FeNi_3$ nanochains. When the amounts of $Fe(acac)_3$:$Ni(acac)_2$ were increased from 0.07:0.2 mmol to 0.17:0.50 mmol (Fe:Ni molar ratio was fixed at 1:3), the sizes of nanospheres in each nanochain increased from 150 to 550 nm in diameter (see Figure I(a−c) in the Supporting Information). This is in response to the increased mass transfer for the growth of the crystal with a higher concentration of the precursor. The molar ratio of Fe:Ni ($Fe(acac)_3$:$Ni(acac)_2$) also play a key role in the morphology of the product. At a molar ratio of 1:0.33, most of the structures were nanospheres. However, when the molar ratio was changed from 1:0.33 to 1:3 (see Figure II(a−f) in the Supporting Information), pure nanochain structures were obtained. In the absence of an iron precursor, pure Ni nanowires were formed (see Figure II(g,h) in the Supporting Information). The effect of solvent was also studied (see Figure III(a,b) in the Supporting Information). When EG was replaced by TEG, ultrafine nanopartiles were obtained.

Figures 2 and 3 reveal that the nanospheres in nanochains are made up of small crystallites and have a rough surface. It is known that a dark blue complex of $[Fe(N_2H_4)_3]^{3+}$ and $[Ni(N_2H_4)_3]^{2+}$ is formed by reacting Fe^{3+} and Ni^{2+} in a hydrazine solution (30), the excess hydrazine reduces the $[Fe(N_2H_4)_3]^{3+}$ and $[Ni(N_2H_4)_3]^{2+}$ complex into Fe and Ni nuclei under microwave irradiation. Here it is because hydrazine is a moderate reducing agent with low cost and has been proved to be good alternative to produce metallic particles (24). Because of the excellent microwave absorbing characteristics of the polar glycol and metallic $FeNi_3$, "hot spots" in the bulk solution and "hot surfaces" on metallic $FeNi_3$ can be created. They would speed up mass transfer and crystal growth. Microwave irradiation would also induce localized ionic currents on the "hot surface" of $FeNi_3$ in an alternating electromagnetic field, providing additional driv-

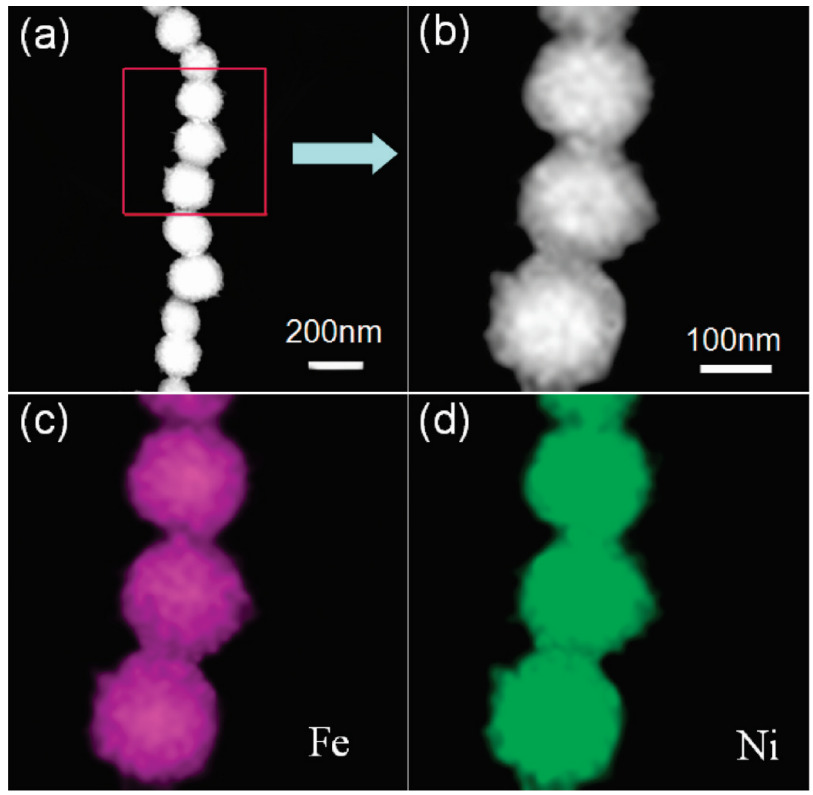

FIGURE 5. (a, b) HAADF-STEM and (c, d) elemental mapping images of a single $FeNi_3$ nanochain.

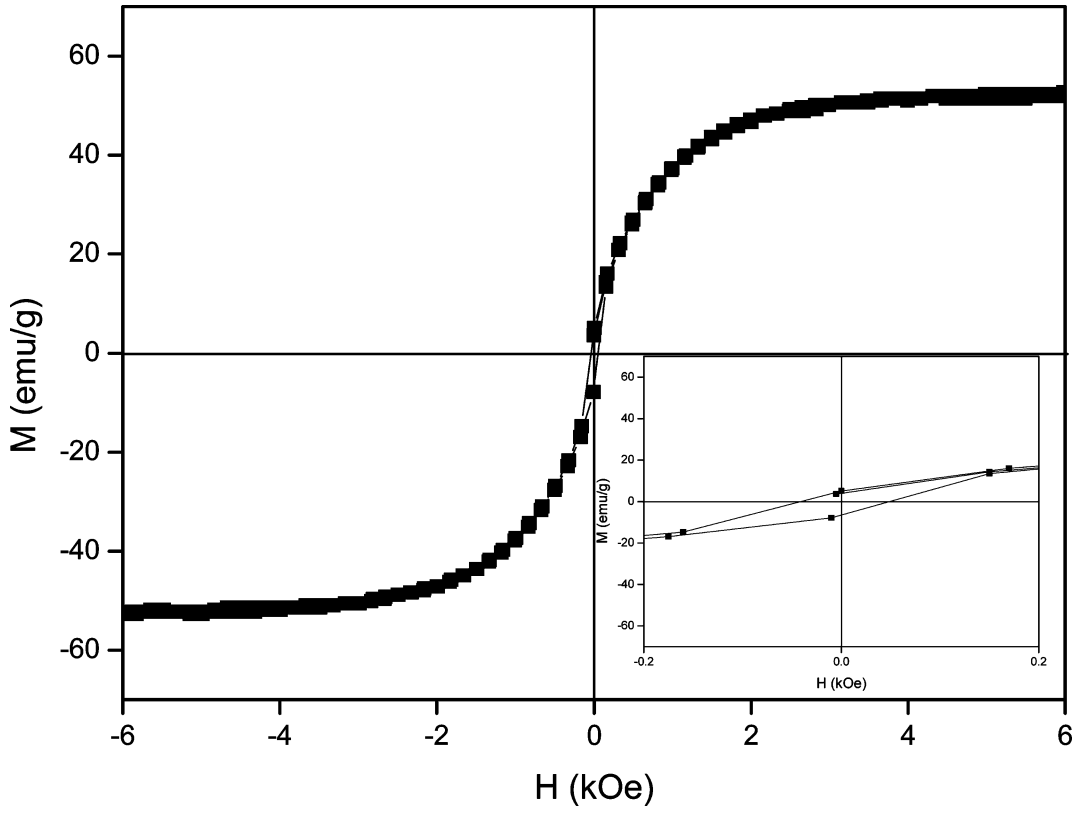

FIGURE 6. Hysteresis loops of the $FeNi_3$ nanochains (S1) at 300 K.

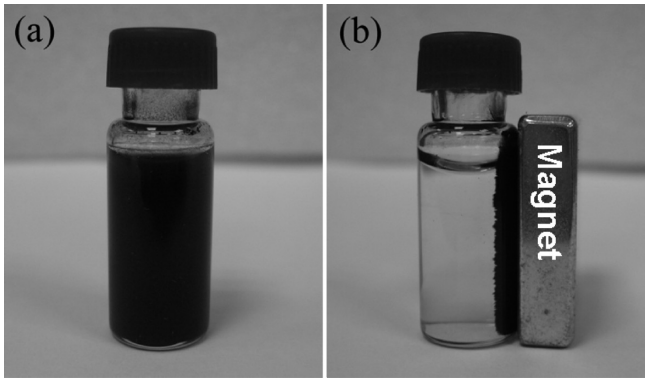

FIGURE 7. (a, b) Photograph of the $FeNi_3$ nanochains dispersed in the water and response to external magnetic field.

ing force for directional crystallographical fusion of nuclei into nanocystals. The crystallites attach to each other, probably driven by the "oriented attachment" mechanism, associate with Ostwald ripening (35), and grow into a chain because of the attractive magnetic forces between the magnetic particles as well as van der Waals interactions (36). The microwave intensity plays a role in the formation of $FeNi_3$ nanochains. A moderate intensity is most appropriate for this synthesis. Decreasing too much the microwave power would slow down reaction rate and affect the purity of the product (37). At very high microwave intensity, the nanoparticle products tend to aggregate (38, 39).

Although rapid development of nanomaterials will certainly continue, the application of some materials may be limited by their inherent toxicity (40, 41). Thus, the need for evaluating nanotoxicity is important. Transparent zebrafish, possessing a high degree of homology to the human genome, offers an economically feasible platform for toxicity assessment of nanomaterials (42). The toxicity of the as-prepared $FeNi_3$ alloyed nanochains were evaluated using zebrafish as a model. Figure IV in the Supporting Information shows in detail the survival rate of zebrafish larvae at different concentrations of nanochains (0, 1, 5, 10, 25, 35, 50 mg/L) after 96 h of exposure. It shows that more than 90% zebrafish larvae survived even under the highest concentration 50 mg/L. Figure V in the Supporting Information shows *in vitro* MRI of $FeNi_3$ nanochains (S1) suspended in DI water at the different concentrations of nanochains (0, 0.001, 0.002, 0.005, 0.01, 0.02, 0.05, 0.1, 0.2 mM). The $FeNi_3$ nanochains resulted in a signal decrease in a concentration-dependent manner, with higher concentration leading to darker signal. The r_2 relaxivity is 70.1 s^{-1} mM^{-1} calculated from Figure VI in the Supporting Information. At TE = 92 ms, the detection limit is 0.002 mM (see Figure V in the Supporting Information), which compared favorably the commercial iron oxide nanoparticles (43, 44). These results demonstrate that this kind of alloy nanochains has the potential to be used as a T_2 MRI contrast agent.

4. CONCLUSIONS

In summary, we have reported a rapid and economical microwave-assisted route to synthesize $FeNi_3$ alloyed nanochains. The diameter of the chains can be tuned by changing the concentration of the precursors, iron(III) acetylacetonate, and nickel(II) acetylacetonate. The prepared $FeNi_3$ alloyed nanochains show enhanced coercivity and saturation mag-

netization. Our preliminary results demonstrated the potential of the new magnetic nanochain for MRI imaging. Much more effort will be needed to develop it into a practical MRI probe. The proposed preparation approach and growth mechanism might be extended to other magnetic substances to direct large-scale synthesis of similar nanochains.

Acknowledgment. This research was supported by a Strategic Investments Scheme administered by The Chinese University of Hong Kong.

Supporting Information Available: Additional figures and tables (PDF). This material is available free of charge via the Internet at http://pubs.acs.org.

REFERENCES AND NOTES

(1) Zhou, Y.; Kogiso, M.; Shimizu, T. *J. Am. Chem. Soc.* **2009**, *131*, 2456–2457.
(2) Gu, Y. X.; Chen, D. R.; Jiao, X. L.; Liu, F. F. *J. Mater. Chem.* **2006**, *16*, 4361–4366.
(3) Jin, Y.; Yang, D. Y.; Kang, D. Y.; Jiang, X. Y. *Langmuir* **2010**, *26*, 1186–1190.
(4) Zeng, J.; Huang, J. L.; Lu, W.; Wang, X. P.; Wang, B.; Zhang, S. Y.; Hou, J. G. *Adv. Mater.* **2007**, *19*, 2172–2176.
(5) Tao, X. Y.; Liu, J.; Koley, G.; Li, X. D. *Adv. Mater.* **2008**, *20*, 4091–4096.
(6) Ariga, K.; Hill, J. P.; Lee, M. V.; Vinu, A.; Charvet, R.; Acharya, S. *Sci. Technol. Adv. Mater.* **2008**, *9*, 014109.
(7) Sudfeld, D.; Wojczykowski, K.; Hachmann, W.; Heitmann, S.; Rott, K.; Hempel, T.; Kammerer, S.; Jutzi, R.; Hutten, A.; Reiss, G. *IEEE Trans. Magn.* **2002**, *38*, 2601–2604.
(8) Kinsella, J. M.; Ivanisevic, A. *J. Phys. Chem. C* **2008**, *112*, 3191–3193.
(9) Goubault, C.; Jop, P.; Fermigier, M.; Baudry, J.; Bertrand, E.; Bibette, J. *Phys. Rev. Lett.* **2003**, *91*, 260802–260805.
(10) Doyle, P. S.; Bibette, J.; Bancaud, A.; Viovy, J. L. *Science* **2002**, *295*, 2237–2237.
(11) Koenig, A.; Hebraud, P.; Gosse, C.; Dreyfus, R.; Baudry, J.; Bertrand, E.; Bibette, J. *Phys. Rev. Lett.* **2005**, *95*, 128301–128304.
(12) Park, J. H.; von Maltzahn, G.; Zhang, L. L.; Schwartz, M. P.; Ruoslahti, E.; Bhatia, S. N.; Sailor, M. J. *Adv. Mater.* **2008**, *20*, 1630–1635.
(13) Leung, K. C. F.; Wang, Y. X.; Wang, H. H.; Chak, C. P.; Cheng, C. H. K. *IEEE Trans. Nanobiosci.* **2009**, *8*, 192–198.
(14) Tremel, W.; Kleinke, H.; Derstroff, V.; Reisner, C. *J. Alloys Compd.* **1995**, *219*, 73–82.
(15) Sun, S. H.; Anders, S.; Hamann, H. F.; Thiele, J. U.; Baglin, J. E. E.; Thomson, T.; Fullerton, E. E.; Murray, C. B.; Terris, B. D. *J. Am. Chem. Soc.* **2002**, *124*, 2884–2885.
(16) Sun, S. H.; Fullerton, E. E.; Weller, D.; Murray, C. B. *IEEE Trans. Magn.* **2001**, *37*, 1239–1243.
(17) Park, J. I.; Cheon, J. *J. Am. Chem. Soc.* **2001**, *123*, 5743–5746.
(18) Kiely, C. J.; Fink, J.; Zheng, J. G.; Brust, M.; Bethell, D.; Schiffrin, D. J. *Adv. Mater.* **2000**, *12*, 640–643.
(19) Chaubey, G. S.; Barcena, C.; Poudyal, N.; Rong, C. B.; Gao, J. M.; Sun, S. H.; Liu, J. P. *J. Am. Chem. Soc.* **2007**, *129*, 7214–7215.
(20) Robinson, I.; Zacchini, S.; Tung, L. D.; Maenosono, S.; Thanh, N. T. K. *Chem. Mater.* **2009**, *21*, 3021–3026.
(21) Datta, A.; Pal, M.; Chakravorty, D.; Das, D.; Chintalapudi, S. N. *J. Magn. Magn. Mater.* **1999**, *205*, 301–306.
(22) Bac, L. H.; Kwon, Y. S.; Kim, J. S.; Lee, Y. I.; Lee, D. W.; Kim, J. C. *Mater. Res. Bull.* **2010**, *45*, 352–354.
(23) Wang, H. Z.; Li, J. G.; Kou, X. L.; Zhang, L. *J. Cryst. Growth* **2008**, *310*, 3072–3076.
(24) Lu, X. G.; Liang, G. Y.; Zhang, Y. M. *Mater. Sci. Eng., B* **2007**, *139*, 124–127.
(25) Liao, Q. L.; Tannenbaum, R.; Wang, Z. L. *J. Phys. Chem. B* **2006**, *110*, 14262–14265.
(26) Tsuji, M.; Hashimoto, M.; Nishizawa, Y.; Kubokawa, M.; Tsuji, T. *Chem.—Eur. J.* **2005**, *11*, 440–452.
(27) Makhluf, S.; Dror, R.; Nitzan, Y.; Abramovich, Y.; Jelinek, R.; Gedanken, A. *Adv. Funct. Mater.* **2005**, *15*, 1708–1715.
(28) Panda, A. B.; Glaspell, G.; El-Shall, M. S. *J. Am. Soc. Chem.* **2006**, *128*, 2790–2791.
(29) Hu, X. L.; Yu, J. C.; Gong, J. M.; Li, Q.; Li, G. S. *Adv. Mater.* **2007**, *19*, 2324–2329.
(30) Yu, J. C.; Hu, X. L.; Li, Q.; Zhang, L. Z. *Chem. Commun.* **2005**, 2704–2706.
(31) Hu, X. L.; Yu, J. C. *Chem. Mater.* **2008**, *20*, 6743–6749.
(32) Hu, X. L.; Yu, J. C. *Chem.—Asian J.* **2006**, *1*, 605–610.
(33) Westerfield, M. *The Zebrafish Book*, 5th ed.; University of Oregon Press: Eugene, OR, 2007; pp 2.1—3.44.
(34) *Water quality—determination of the actual lethal toxicity of substances to a freshwater fish [Brachydanio rerio Hamilton-Buchanan (Teleostei, Cyprinidae)] Part 2: Semi-static method*; ISO 7346-2; International Organization for Standardization: Geneva, Switzerland, 1996.
(35) Murphy, C. J.; Jana, N. R. *Adv. Mater.* **2002**, *14*, 80–82.
(36) Huelser, T. P.; Wiggers, H.; Ifeacho, P.; Dmitrieva, O.; Dumpich, G.; Lorke, A. *Nanotechnology* **2006**, *17*, 3111–3115.
(37) Han, J. K.; Song, H. Y.; Saito, F.; Lee, B. T. *Mater. Chem. Phys.* **2006**, *99*, 235–239.
(38) He, Y. J. *China Part.* **2004**, *2*, 168–170.
(39) Jiang, Z. L.; Feng, Z. W.; Shen, X. C. *Chin. Chem. Lett.* **2001**, *12*, 551–554.
(40) Oberdorster, G.; Oberdorster, E.; Oberdorster, J. *Environ. Health Perspect.* **2005**, *113*, 823–839.
(41) Grainger, D. W.; Castner, D. G. *Adv. Mater.* **2008**, *20*, 867–877.
(42) Bar-llan, O.; Albrecht, R. M.; Fako, V. E.; Furgeson, D. Y. *Small* **2009**, *5*, 1897–1910.
(43) Wang, Y. X.; Hussain, S. M.; Krestin, G. P. *Eur. Radiol.* **2001**, *11*, 2319–2331.
(44) Corot, C.; Robert, P.; Idée, J. M.; Port, M. *Adv. Drug Delivery Rev.* **2006**, *58*, 1471–1504.

AM100410R